Bull Earthquake Eng (2012) 10:211–234
DOI 10.1007/s10518-010-9216-4

ORIGINAL RESEARCH PAPER

Calibration and application of a continuum damage model on the simulation of stone masonry structures: Gondar church as a case study

Bruno Silva · João M. Guedes · António Arêde · Aníbal Costa

Received: 13 July 2009 / Accepted: 30 October 2010 / Published online: 21 November 2010

Abstract The conservation and rehabilitation of monuments is a matter of important investigation, and the need for accurate structural analysis, capable of effectively predicting the structural behaviour of this type of constructions, under static and dynamic loads, is increasing. Currently there are numerous computational methods and tools, supported by different theories and strategies with different levels of complexity, computation time and cost which are available to perform such analyses. A complex analysis is not always synonym of a better result and the choice of a method over another depends mostly on the purpose of the analysis. This work aims at evaluating the capacity of a non linear continuum damage model (Faria et al. in Int J Solids Struct 35(14):1533–1558, 1998), originally developed for concrete structures, to simulate the behaviour of stone masonry structures. In particular, the seismic response of an old stone masonry construction, the Gondar church, is analysed considering different levels of geometrical and material complexity. The verification and calibration procedures use the experimental results from tests performed on stone masonry walls at the Laboratory for Earthquake and Structural Engineering of the Faculty of Engineering of Porto University and from other tests found in the bibliography (Vasconcelos in Experimental investigations on the mechanics of stone masonry: Characterization of granites and behaviour of ancient masonry shear walls. PhD Thesis, Universidade do Minho, Guimarães, Portugal, 2005). The results are compared, assessing the differences and the importance of using complex tools,

B. Silva (✉) · J. M. Guedes · A. Arêde
Department of Civil Engineering, Faculty of Engineering, University of Porto, R. Dr. Roberto Frias s/n, 4200-465 Porto, Portugal
e-mail: silva@dic.unipd.it

J. M. Guedes
e-mail: jguedes@fe.up.pt

A. Arêde
e-mail: aarede@fe.up.pt

A. Costa
Department of Civil Engineering, University of Aveiro, Campus Universitário de Santiago, 3810-193 Aveiro, Portugal
e-mail: agc@fe.up.pt

such as the continuum damage model, to better simulate and understand the global behaviour of such constructions.

Keywords Stone masonry · In-plane behaviour · Numerical modelling · Continuum damage model · Sensitivity analysis · Seismic analysis

1 Introduction

Masonry is one of the oldest "structural materials" still in use. It has been used on a large variety of constructions, either common or monumental, many classified as cultural and architectural heritage. The preservation and valorisation of this legacy through active and integrated interventions is nowadays seen as a cultural matter.

Masonry is by nature a heterogeneous material, whose components present a quite unknown geometry and a high variability of the mechanical properties. Therefore, a great effort has been done in order to gather further knowledge. Experimental studies performed either in laboratory (Tomaževic 1992; Corradi et al. 2003; Vintzileou and Tassios 1995; Vasconcelos 2005) and in situ (Corradi et al. 2002; Costa et al. 2010) complemented by NDT and SDT campaigns using flat-jacks, sonic equipment, dynamic identification procedures, among other techniques (Binda et al. 1997; Valluzzi et al. 2001), constitute an important source of information, in particular for the development and calibration of numerical tools able to predict the behaviour of masonry structures.

The finite element method is one of the most powerful approaches to simulate masonry structures. The method can be applied to different detailed levels, from micro to macro, depending on the objectives set for the analyses. Works like those presented in Betti et al. (2006), Silva et al. (2007) and Costa et al. (2006) follow a detailed micro modeling strategy for masonry, being the material divided into its basic components: joints, blocks and infill. Such modelling strategy not only requires an "exact" knowledge of the masonry structure, as it involves a high modelling and computation time and effort, making it impracticable for simulating real constructions. This kind of modeling is only adequate for studying local effects on restricted parts of a structure and it requires the detailed knowledge of the material and geometrical characteristics of the masonry constituents.

Authors, like Gambarotta and Lagomarsino (1997a) and Lourenço and Rots (1997a), propose simplified micro modelling strategies, characterized by the combination, or omission of certain constituents, allowing a drastically reduction of the computation time without important loss of accuracy.

Still on the finite elements domain, masonry can be simulated using mechanical macro models, also known as homogeneous or continuous, in which all the masonry composing elements are merged into a continuous mass (Lourenço et al. 1997b; Gambarotta and Lagomarsino 1997b). The relation between masonry average stresses and extensions is established by adopting a phenomenological standpoint or homogenization techniques. Although developed for the study of concrete elements, the continuum damage model presented in Faria et al. (1998) is a good example of these type of models. However, due to the masonry particular characteristics, these models present limitations, which some authors have tried to overcome through modifications with some success (Saetta et al. 2000; Berto et al. 2001; Cervera 2003).

The use of these models gains special importance when analysing structures located on high seismic hazard areas, being an essential tool for the characterization of seismic vulnerability levels and for the definition of effective rehabilitation procedures, i.e., interventions with

adequate technical and financial planning that will allow rehabilitation and (or) strengthening measures capable of minimizing damage and avoiding human and physical losses (Vicente et al. 2007; Penazzi et al. 2001). In particular, these analyses allow the construction of seismic risk maps for buildings, correlating seismic risk to damage prediction (Valluzzi et al. 2004).

This work aims at evaluating the capacity of a non linear continuum damage model (Faria et al. 1998) originally developed for concrete structures, to simulate the behaviour of stone masonry structures, i.e., structures of heterogeneous nature and anisotropic behaviour. In this model, the various components of the stone masonry walls: rocks, infill and joints are considered as part of a unique and homogeneous material. The first part of the work refers to the model calibration procedures. This process consists on fitting a series of experimental results from tests performed on stone masonry walls at the Laboratory for Earthquake and Structural Engineering (LESE) of the Faculty of Engineering of Porto University (FEUP), and from tests found in the literature (Vasconcelos 2005), with the model. The experimental tests performed at the LESE are described in detail in Sect. 2.

Afterwards, the seismic response of an old stone masonry construction, Gondar church, is analysed using the continuum damage model. The analyses consider different modelling strategies based on different degrees of geometrical complexity, different finite elements (shells and volumes) and different behaviour models (linear elastic or non linear continuum damage). The results of the different modelling strategies, namely the stresses and deformation state of the masonry walls and the identification of the most vulnerable spots, are analysed and compared to assess the differences and the importance of using complex tools to better simulate and understand the global behaviour of such constructions. The simulations are done using the finite element software Cast3M (CEA 1990).

2 Experimental test campaign on two stone masonry walls (LESE)

A stone masonry wall is a composite element made of stones, mortar joints and internal filling material. It's a highly heterogeneous structural element as, in general, its constituents present irregular geometry and large dispersion on the mechanical properties. Studies have been done in the past and are still being done to identify, in the middle of this diversity, groups with similar geometrical characteristics / morphology (cross-section, elevation, number and thickness of leaves, technical and constructive measures, etc.) and mechanical properties (Roque 2002; Binda et al. 1997). Such standardization is of great importance and will help technicians to intervene on old stone masonry constructions following more sustainable approaches. In-situ and laboratory testing campaigns gives essential data to this characterization. Moreover, they also allow improving and calibrating numerical tools and mechanical models to the structural analysis of this type of constructions.

2.1 Walls description

Several masonry walls have been tested under compressive and shear forces at the LESE (Costa et al. 2006; Silva et al. 2007). In particular, two irregular stone masonry walls (PA1 and PA2) were constructed for that purpose and the results were later used to calibrate the continuum damage model used in this work. The specimens are two leaves irregular granite masonry walls: 0.6 m thick, 1.6 m long and 1.6 m high, i.e. two short walls with an aspect ratio of 1 (ratio between height and length). The two leaves are made of good quality granite stones. The stones were positioned in layers along both sides/leaves using clay mortar. Some stones were positioned along the transverse direction of the walls to connect the leaves and

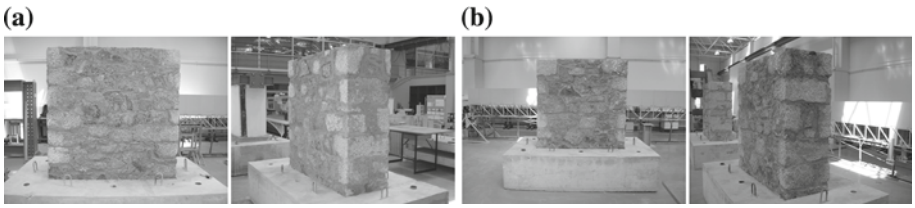

Fig. 1 Tested walls: **a** PA1 and **b** PA2

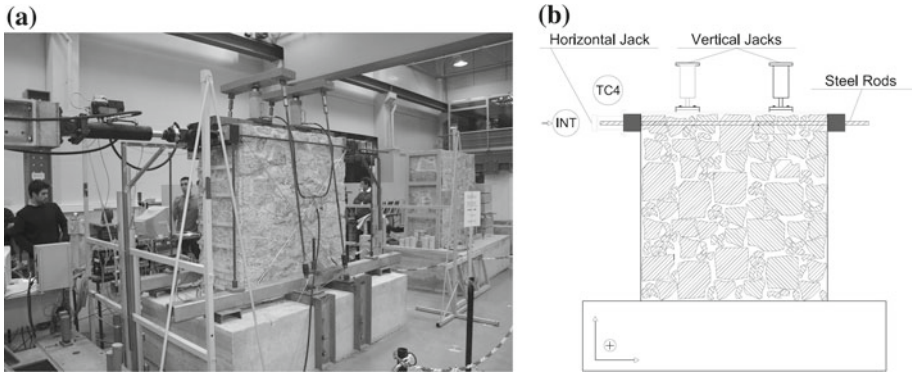

Fig. 2 Test setup

improve the global behaviour. This is a reliable construction procedure commonly used on multiple leaves masonry walls. The walls were built on a $(1.6 \times 2.6 \times 0.6)$ m^3 concrete block that simulates the foundation, with a fixing depth of 0.35 m (Fig. 1).

2.2 Test setup

The walls were submitted to a constant vertical load and controlled horizontal in-plane cyclic displacements. The horizontal load was applied to the top of the walls through a hydraulic jack with hinges at the edges and using a vertical steel reaction structure. To guarantee a uniform distribution of the horizontal load, the two opposite lateral faces of the walls were connected at the top using steel rods (Fig. 2). The vertical force (50.0 kN, corresponding to a compression stress of approximately 52.0 kPa) was applied to the top by means of two smaller hydraulic jacks to simulate the weight of the structure that should exist above the specimens. Each of the jacks was set against a steel beam connected to the concrete foundation block through two steel rods. The vertical load sought to simulate the existence of structures/loads above the wall, in particular the mass of a wooden roof structure and a 1.9 m high wall, reproducing a wall recovered from a one floor 3.5 m high house. The foundation block was connected to the laboratory reaction floor via four monitored high strength pre-stressed rods to avoid any displacement of the block during the test.

The tests on PA1 and PA2 and referred to PA1NR and PA2NR, were performed using a displacement control system that simultaneously acquired data from all monitored points. The displacements were imposed with increasing amplitude, up to 12.0 mm; each displacement cycle was repeated three times (Fig. 3). The wall was monitored using nine load cells, one at each of the four steel rods transferring the vertical reaction force to the foundation block, one at each of the four steel rods connecting the foundation block to the

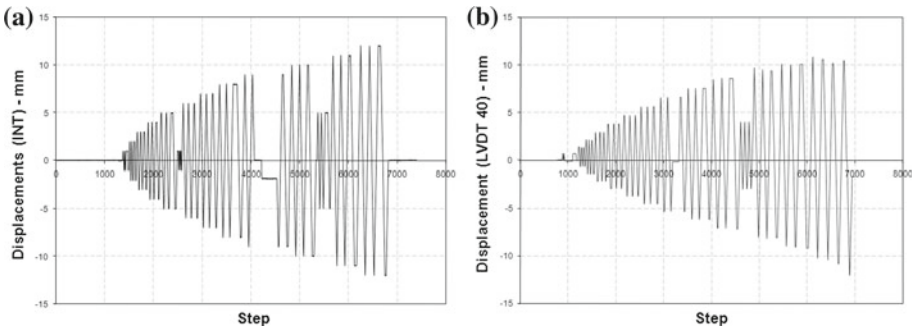

Fig. 3 Horizontal displacements applied to the top of the walls: **a** test PA1NR and **b** test PA2NR

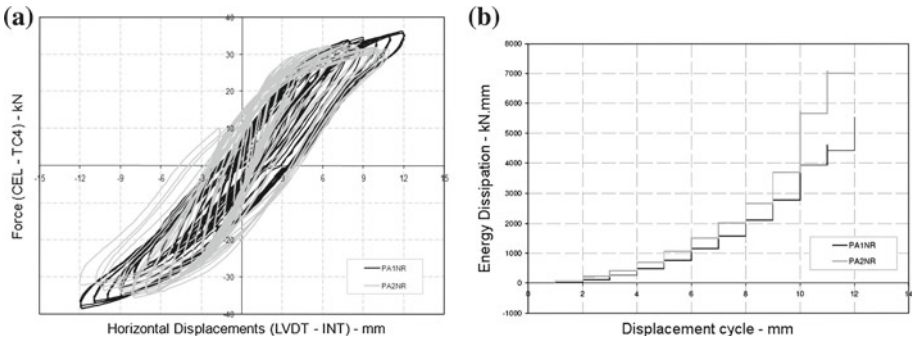

Fig. 4 Global experimental results (PA1NR and PA2NR): **a** horizontal force (TC4) vs. horizontal displacement applied to the top of the walls (INT) and **b** evolution of the dissipated energy along the test

laboratory floor and one at the horizontal actuator (TC4). The horizontal displacements on the top of the walls were monitored through internal displacement transducers (INT) (Fig. 2).

2.3 Experimental results

2.3.1 Global behaviour

The global behaviour response curves (applied horizontal force vs imposed horizontal displacement) and the quantification of the energy dissipation for both walls are presented in Fig. 4a and b, respectively. The maximum imposed displacement of 12.0 mm corresponds to a drift of 0.75% and to a displacement ductility at the top of approximately 2. Notice that pronounced plastic behaviour was avoided during the test, since the walls were meant to be repaired/strengthened and tested again later.

According to the obtained experimental results it is possible to conclude that:

- Both walls present a similar response curve in both loading directions with a slight difference in terms of maximum strength that is slightly higher for PA1 wall;
- For the different levels of imposed displacement there wasn't a significant loss of stiffness. In both walls the inclination of the loading and unloading paths in both loading directions is similar and identical to the initial loading cycle;
- The walls reveal some capacity to dissipate energy through hysteretic behaviour, i.e., due to the non linear behaviour. This capacity is particularly important when the structures

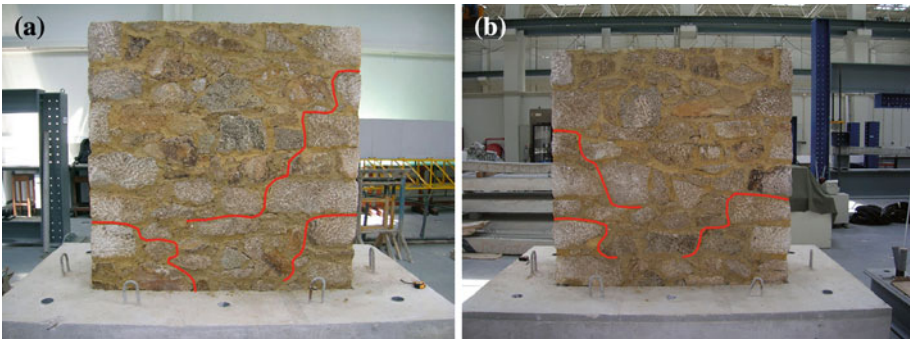

Fig. 5 Damage pattern on PA1 after the test: **a** frontal face and **b** back face

are subjected to dynamic loads, namely seismic, avoiding major damage accumulation in the structure. The capacity to dissipate energy is higher for PA2;

- In the final phase of the experimental tests, the walls started exhibiting considerable non linear plastic deformation and higher energy dissipation and, in the case of PP2, loss of resistance.

The capacity to dissipate energy is an important aspect of the dynamic behaviour of structures, being associated to a decrease on the seismic response. The dissipated energy can be evaluated in a qualitative way through the correlation between applied force and sustained displacement, while its quantitative estimation can be obtained for each of the hysteretic cycles of displacement by the numerical integration of the force vs displacement curve. As illustrated in Fig. 4b, the dissipated energy in both experimental tests increases exponentially with the increase of the imposed displacement. It is associated to the increase of damage in the structure; initially the increase of dissipated energy is not very pronounced because damage still isn't relevant, but as the imposed displacement increases, i.e., as new cracks appear, in particular diagonal cracks, it becomes more pronounced and visible. Notice that although the walls are similar in terms of constructive method, materials and geometric features, they show differences in the total dissipated energy of approximately 27.0%. This is mainly justified by local phenomena that occur during the tests which are random in nature and specific to each of the tested structures. The definition of an average value for dissipated energy, consensual and reliable to be accepted in the study of such walls, needs a larger number of experimental tests.

2.3.2 Local behaviour

Figures 5 and 6 present the damage patterns on the walls after the tests, in particular the main cracks (joint openings) underlined in black.

As can be seen in the previous figures, the damage patterns indicate that the walls respond with a behaviour dominated by bending with damage mainly concentrated near the base and some distribution along the height. As the horizontal displacement increases, shear behaviour gains a more important role that is confirmed by the opening of joints along the diagonals.

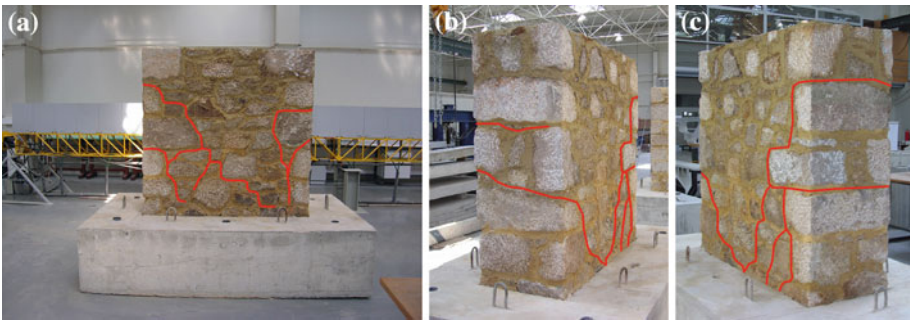

Fig. 6 Damage pattern on PA2 after the test: **a** frontal face **b** lateral and **c** back face

2.3.3 General comments

The two tests allowed assessing the cyclic behaviour of this type of structures and the phenomena, local and global, involved. In the course of the tests it was possible to observe the way the walls deformed and where and how damage concentration areas (cracking and joints opening) appeared and developed along the structure. Besides, the tests allowed determining global parameters such as the stiffness (loading, unloading and reloading), the energy dissipation and the resisting capacity of the structure.

The heterogeneity of this material commands the local behaviour observed in the tests; the results are quite sensitive to the way the stones and joints are distributed, with concentration of damage at the joints. However, at global level the walls responded with great symmetry and uniformity, diluting many of the local particularities. The walls responded with an overall in-plane non linear behaviour with relative ductility and ability to dissipate energy, i.e., in-plane seismic resisting capacity. Notice that most of the resisting capacity of these specimens is constrained by the static equilibrium between the destabilizing moment, generated by the horizontal action, and the stabilizer moment introduced by the vertical action; experimental tests conducted in walls with similar geometry, and the same level of vertical load, will respond with similar resisting capacity.

This study reports only to the in-plane behaviour of stone masonry walls; the out-of-plane behaviour of these structures may present quite different characteristics, being largely influenced by other structural elements, such as transversal walls, floors and roof elements.

Finally, this experimental campaign, besides allowing a better understanding of the walls structural behaviour, is also used in Sect. 3 to verify and calibrate the continuum damage model for simulating stone masonry structures.

3 Continuum damage model: calibration

3.1 Introduction

The non linear Continuum Damage Model (Faria et al. 1998) adopted in this study to simulate stone masonry relies, like any other existing computational approaches, on simplifications. In the case of this model, it assumes the material is homogeneous and isotropic. Although it is far from reality, the consideration of homogeneity is the most feasible way to represent a complex material like stone masonry, where stones, joints and infill have an unknown geometry and

distribution. Furthermore, even if that knowledge existed, the necessary detail would make the simulation of a real construction impracticable. Notice that the large dimensions involved on such a structure contribute to transform this complex geometry into a more homogeneous material. As for the isotropic aspect, although it doesn't represent properly stone masonry, the model induces anisotropy through damage distribution and generates preferential rupture lines.

3.2 General considerations: Continuum damage model

The Continuum Damage Model (Faria et al. 1998) was originally developed for the analysis of large dimension concrete structures such as dams and it is capable of reproducing the dissimilar degrading phenomena that occurs under tension or compression. The model incorporates two damage variables; one for tension $\left(d^{+}\right)$ and another for compression $\left(d^{-}\right)$ and a plastic deformation tensor for the characterization of the non linear concrete degradation mechanisms under tensile and compression conditions. In reality, the concept of damage can be interpreted as a measure of defects, micro-cracks micro-cavities developed in the material elements, being the non linearity of the material behaviour a consequence of the evolution of those same defects.

The model constitution is capable of reproducing the material stress / deformation curves, including hardening and softening effects and the mechanisms for recovery of stiffness. In the field of Damage Mechanics, the effects of damage on the material properties initially elastic are reproduced in the stiffness constitutive tensor. The damage is reflected in the reduction of several of the stiffness components, and the damaged material may remain isotropic or become anisotropic.

The damage variables $\left(d^{-}\text{and } d^{+}\right)$ can only assume values between 0 and 1 (1); 0 corresponds to the elastic state and it increases with the evolution of the damage until it reaches 1 that corresponds to the collapse state. This evolution is characterized by the decrease of the effective resistant area, i.e., area without defects. The damage variables show three types of laws, depending on whether the analysis of damage is in tensile, in compression or in cyclical conditions. These laws are obtained by experimental observation, being dependent on hardening variables that depend on the deformation of the element.

$$0 \leq \left(d^{+}, d^{-}\right) \leq 1 \tag{1}$$

A basic entity of such a model is the "effective stress tensor" $(\overline{\sigma})$ which is split into tensile $(\overline{\sigma}^{+})$ and compressive $(\overline{\sigma}^{-})$ components in order to clearly distinguish the respective stress contributions. In what concerns the constitutive law, the model leads to the following intuitive format:

$$\sigma = \left(1 - d^{+}\right)\overline{\sigma}^{+} + \left(1 - d^{-}\right)\overline{\sigma}^{-} \tag{2}$$

In the need to define, with precision, if the element is in "load", "unload" or "reload" condition the model introduces the concept of equivalent tension associated to a positive scalar value, which is the result of the norm of tensors of effective tensions. The different three-dimensional states of tension can then be compared through a 1D analysis. Following the tensor decomposition adopted by this model, the equivalent tensile and compressive tensions are then considered, being associated with different damage criteria.

As explained by Faria (1994) the constitutive law (2) becomes quite perceptible when applied to tensile or compression 1D tests in which one of the components is always zero, thus reducing the constitutive law to the scalar equations (3) and (4), according to the type of test (tensile or compression) and to the curves in Fig. 7.

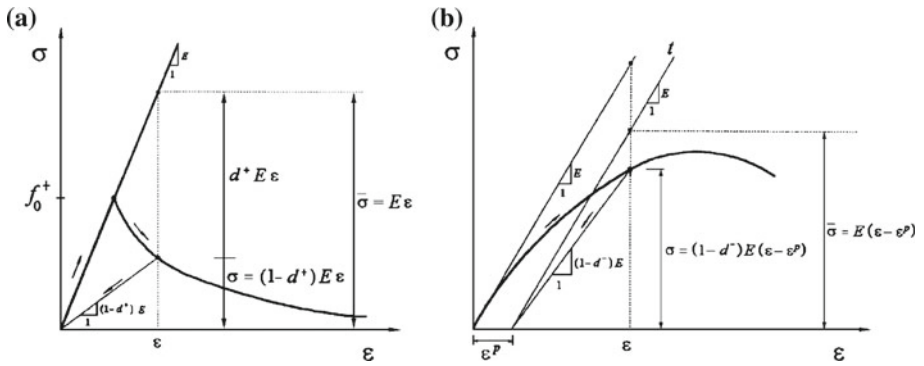

Fig. 7 Material behaviour (Faria 1994): **a** uni-axial traction and **b** uni-axial compression

$$\text{Uni-axial tensile test}: \quad \sigma = \left(1-d^+\right)\overline{\sigma}^+ = \left(1-d^+\right)\cdot E\cdot\varepsilon \tag{3}$$

$$\text{Uni-axial compressive test}: \quad \sigma = \left(1-d^-\right)\overline{\sigma}^- = \left(1-d^-\right)\cdot E\cdot\left(\varepsilon-\varepsilon^p\right) \tag{4}$$

As it can be seen in Fig. 7a, in traction the effective elastic tension $\overline{\sigma}^+ = E\cdot\varepsilon$ is converted into real tension (σ) directly through factor $\left(1-d^+\right)$ and the unloading is made to the origin through a secant modulus $E' = \left(1-d^+\right)E$. In compression (Fig. 7b), the effective tension ($\overline{\sigma}^-$) in a particular point is given by the product of the elastic elasticity modulus (E) by the strain (ε) on that point affected by the plastic strain (ε^p). The real tension is given by the value of real effective tension affected by factor $\left(1-d^-\right)$. The unloading is not made to the origin, creating plastic strain.

To apply this numerical model on the simulation of a stone masonry structure it is assumed that initially, i.e., before the application of any load or load cycle, the material is isotropic and homogeneous. All the numerical simulations under this work have been performed using the finite elements program Cast3M where this continuum damage model is also implemented (Costa 2004).

3.3 Calibration and verification based on the experimental campaigns

The calibration of this or any other model is an important preliminary phase of the numerical simulation of a structure. This paper deals both with the calibration and verification of the efficiency of the continuum damage model to simulate stone masonry structures. In particular, constitutive models contain parameters that must be quantified based on experimental tests. Some of these parameters can be determined explicitly through standardized tests to determine average acceptable values; others can be obtained considering the direct fitting between numerical and experimental global behaviour curves. It is known that the problem of parameter identification corresponds to the optimisation of its estimative through a reverse process, where the deviations between the experimental and the numerical curve are minimized. Such a process requires experimental results as starting point, and may involve the use of linear or non linear error treatment methods in the optimization of the estimative.

The continuum damage model was calibrated using the experimental results obtained in the experimental campaign performed on the masonry walls PA1 and PA2 and, afterwards, in the experimental campaign found in Vasconcelos (2005). With this type of model the walls don't need to be discretized in their basic components (stone blocks, infill and joints),

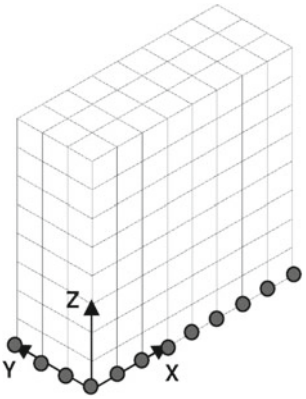

Fig. 8 Numerical model of the walls PA1 and PA2

but in a unique homogenized material. Therefore, only the external dimensions of the walls are needed to generate the geometric model. The finite elements meshes were built using auxiliary programmes, created on purpose, that convert the geometry defined in AutoCAD (Autodesk 2002) into meshes completely characterized and ready to be computed in gibiane language (.dgibi) used by Cast3M.

3.3.1 Calibration based on experimental results (LESE)

The walls PA1 and PA2 were defined in Cast3M by an $8 \times 8 \times 3$ regular mesh composed by 192 volumetric 8 node elements and a mesh density of 0.2 in the three directions (Fig. 8). The numerical walls were fixed at the basement. To reproduce the experimental tests, the same vertical load (50.0 kN) and horizontal displacements law used in the experiments (Fig. 3) were imposed at the top of the walls.

The calibration of the model was done through direct fitting of the numerical curves to the experimental ones (horizontal force vs. displacements measured at the top of the walls), paying particular attention to the stiffness, strength and loading and unloading trajectories. In the case of parameters directly linked to the mechanical properties, it was required to respect the range of values found in the literature. Furthermore, the deformations due to sliding along the joints, which were observed during the tests, were considered by "decreasing" the material stiffness. Finally, to capture the experimental behaviour of the structure, mainly at the first loading cycles, a low tensile strength was considered; the characteristics that define the tensile branch of the material behaviour curve were chosen to confer to the stone masonry fragile low strength behaviour, with an exponential post-peak softening behaviour law.

Taking all this into account, a set of parameters was selected (see Table 1), and the corresponding numerical material behaviour curve is presented in Fig. 9, while Fig. 10 presents the comparison between the numerical and the experimental response curves. The results show that the calibration based on the experimental results of the walls PA1 and PA2 allowed a good fit to the global experimental response curves of both walls in terms of strength and initial loading stiffness. However, even in the case of this phenomenological fitting the model wasn't able to adequately represent the loading and unloading stiffness along the different

Table 1 Numerical parameters from the calibration based on the results from experimental tests on the walls PA1 and PA2

Parameters	Definition	Values	Units
EXTP	Reference strain for plastic parameter	−0.15	–
STRP	Reference stress for plastic parameter	−1.70	MPa
EXT1	Fitting point 1 and 2 (strain)	0.084	–
EXT2		−0.15	–
STR1	Fitting point 1 and 2 (stress)	−2.00	MPa
STR2		−1.7	MPa
YOUN	Young modulus	0.1	GPa
NU	Poisson coefficient	0.25	–
RHO	Specific mass	2200	kg/m^3
NCRI	Tensile softening criteria	1	–
FTU1	Tensile strength	0.10	MPa
REDC	Drop factor for peak tensile stress	0.0	MPa
FC01	Elastic limit compressive stress	−0.30	MPa
RT45	Equi-biaxial compressive ratio	1.0	–
EXTU	Ultimate limit strain	−0.18	–
FCU1	Compressive strength	−2.30	MPa
HLEN	Effective length	Dens = 0.2	
GVAL	Fracture energy	50.0	J

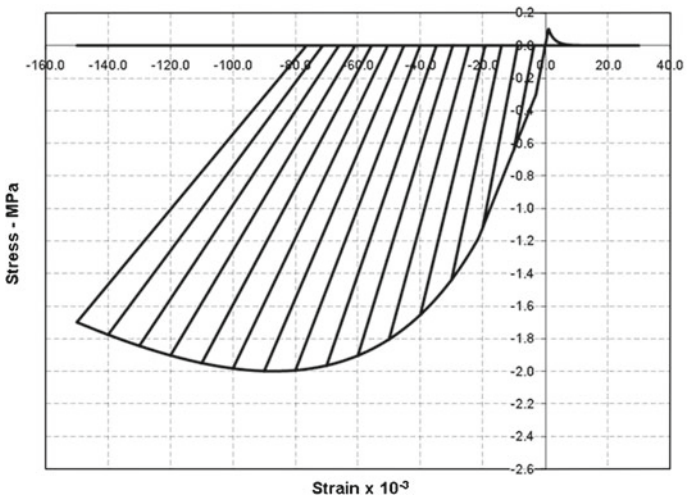

Fig. 9 Numerical material behaviour curve for stone masonry—calibration based on the results from experimental tests on PA1 and PA2

cycles and, consequently, the energy dissipation of the walls. However, and although the differences, the results show that the model has enough potential to be used on the simulation of stone masonry walls, both under static and dynamic loads.

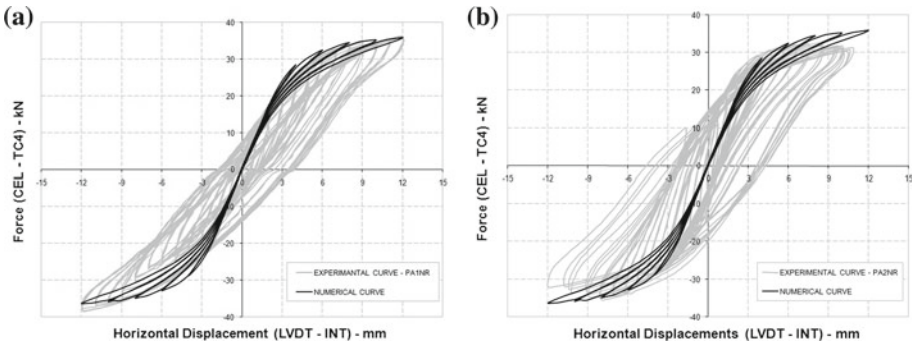

Fig. 10 Comparison of the walls experimental and numerical behaviour response curves: **a** test PA1NR and **b** test PA2NR

3.3.2 Calibration based on a bibliographical case

After this first model calibration and evaluation, the procedure was repeated using now the results of an experimental campaign found in Vasconcelos (2005). The campaign consisted on a series of tests, both on the masonry and on its components to characterize the mechanical behaviour of stone masonry walls. Based on these results, namely on compression tests on irregular masonry columns $(0.15 \times 0.15 \times 0.49)\,m^3$ made by granite stones overlaid with lime mortar joints, a new calibration and evaluation of the continuum damage model was performed by calibrating directly the compression branch of the material behaviour curve. The parameters adopted for the tensile branch were those considered for the walls PA1 and PA2 in Table 1. This procedure gave as output the parameters presented in Table 2 that corresponds to the numerical material behaviour curve presented in Fig. 11.

The continuum damage model was then applied, considering the parameters in Table 2, on the simulation of shear-compression in-plane tests on a series of irregular stone masonry walls $(0.2 \times 1.0 \times 1.2)\,m^3$ presented in Vasconcelos (2005). The simulation of these tests in Cast3M was then performed as described in the previous section.

The walls (WI) were tested under two levels of constant axial force (100 and 250 kN), each one applied to two different walls and considering the horizontal displacement time history law described in Vasconcelos (2005). The response of the walls in terms of in-plane top horizontal force versus displacements is presented in Fig. 12; Table 3 presents the experimental failure modes of these same walls.

The cyclic behaviour of the walls subjected to low levels of pre-compression, WI_1-100 kN and WI_2-100 kN, was essentially governed by a rocking mechanism that is visible in the S shape exhibited by the force versus displacement diagrams of the walls, Fig. 12a and b. Horizontal cracks developed at the base of the walls, which progressively spread along its height.

The cyclic behaviour of the walls submitted to the highest level of pre-compression, WI_1-250 kN and WI_2-250 kN, was dominated by flexure. In this case the rocking mechanism takes a minor role in the global lateral response. The graphs at Fig. 12c and d show that for moderate deformation levels there is some dissipation of energy, which becomes particularly significant after peak load is reached in case of wall WI_2-250 kN and to minor extent in case of wall WI_1-250 kN. This is directly related to the strength and stiffness degradation beyond the peak load, which is due to progressive degradation of the toes of the wall. Although wall WI_2-250 kN fails due to toe crushing, the failure was not explosive, enabling to capture the post-peak regime. In turn, the toe crushing of the wall WI_1-250 kN is followed by a signifi-

Table 2 Numerical parameters from the calibration based on the results found in Vasconcelos (2005)

Parameters	Definition	Values	Units
EXTP	Reference strain for plastic parameter	−0.022	–
STRP	Reference stress for plastic parameter	−3.30	MPa
EXT1	Fitting point 1 and 2 strain	−0.0132	–
EXT2		−0.0157	–
STR1	Fitting point 1 and 2 stress	−2.46	MPa
STR2		−2.37	MPa
YOUN	Young modulus	1.30	GPa
NU	Poisson coefficient	0.25	–
RHO	Specific mass	2200	kg/m^3
NCRI	Tensile softening criteria	1.0	–
FTU1	Tensile strength	0.10	MPa
REDC	Drop factor for peak tensile stress	0.00	MPa
FC01	Elastic limit compressive stress	−0.80	MPa
RT45	Equi-biaxial compressive ratio	1.0	–
EXTU	Ultimate limit strain	−0.0245	–
FCU1	Compressive strength	−26.30	MPa
HLEN	Effective length	Dens = 0.2	
GVAL	Fracture energy	50.0	J

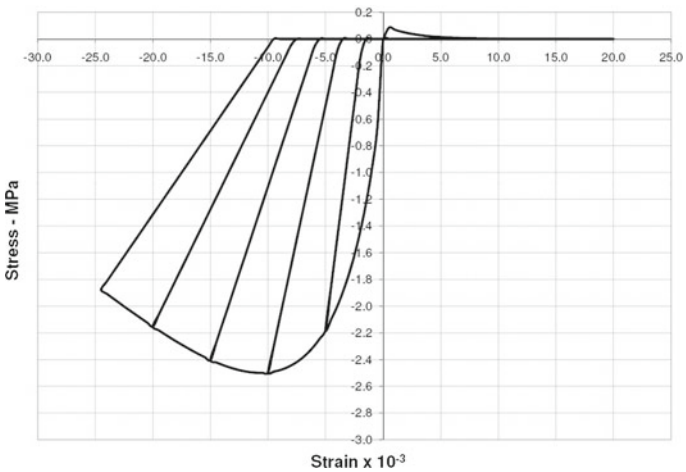

Fig. 11 Numerical material behaviour curve for stone masonry—calibration based on the results from the literature (Vasconcelos 2005)

cant reduction of the lateral resistance and a remarkable loss of lateral stiffness. Notice that a reduction in deformation capacity was found for the walls under higher pre-compression level.

Figure 12 also illustrates the comparison between the experimental and the numerical results. The constitutive model was able to reproduce the experimental curves when the rocking mechanisms governed the walls behaviour. However, the shear failure modes were hardly captured by the model, which responded with lower dissipated energy.

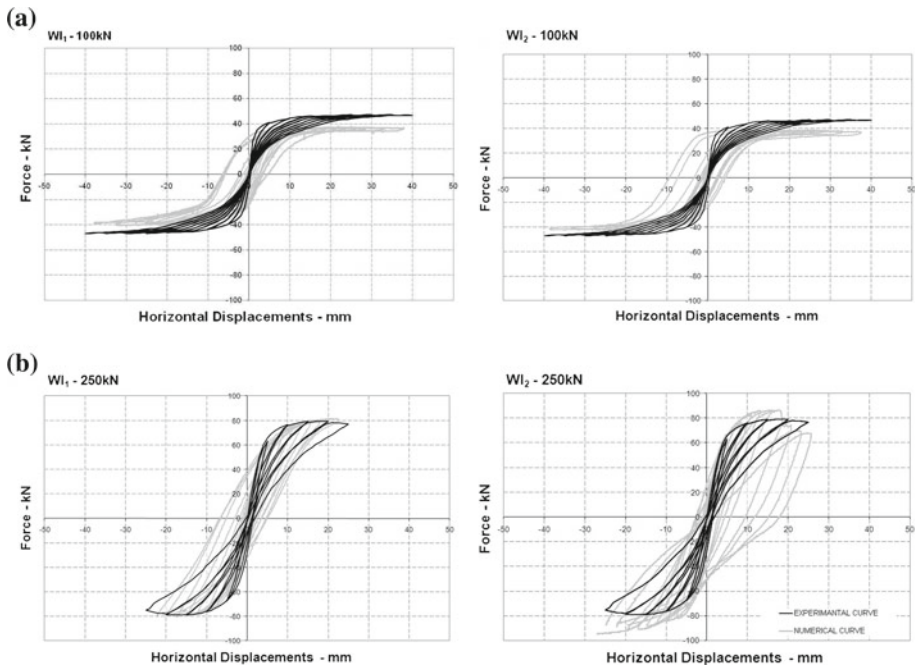

Fig. 12 Comparison of the walls experimental and numerical behaviour response (in-plane top horizontal force vs. displacement) for 2 levels of axial force: **a** 100.0 kN and **b** 250.0 kN

Table 3 Summary of the failure modes of irregular masonry walls (Vasconcelos 2005)

Walls	Failure mode
WI_1-100	Flexural/rocking
WI_2-100	Flexural/rocking
WI_1-250	Flexural/toe crushing
WI_2-250	Flexural/shear/toe crushing

3.4 Conclusions

The results of the two calibration procedures show that the pre-compression stress applied to the walls tested by Vasconcelos is higher than the one applied to the walls tested at the LESE, and that this induced a better fitting between the numerical and the experimental results. However, the same difficulties in simulating the unloading stiffness and the energy dissipation were observed in the two cases. This is mainly due to the inability of the model to capture phenomena related to the walls local behaviour, such as the joints friction.

As final conclusion one can say that, although the damage model is capable of capturing the main global phenomena of stone masonry walls, the local behaviour, which is highly dependent on the geometrical features, can be hardly simulated with such a homogenous model. In particular, the model can't represent the sliding along the joints, which induces highly non linear shear behaviour. However, these phenomena should decrease in importance with the increase of the walls dimension when compared to the dimension of the composing elements (stones).

Fig. 13 The Gondar church

4 Case study: Gondar Church

4.1 Church description

The Gondar church (Fig. 13) is a beautiful but discrete example of religious, Romanic architecture, located on Gondar village near Amarante on the North region of Portugal. This church, also known as Gondar monastery, is in fact what's left of a Benedict monastery founded on the twelfth century. After being abandoned and in ruin for many years, in 1978 the church was classified as Property of Public Interest and was registered in the Architecture Heritage Inventory of the General Directorate of Buildings and Monuments of Portugal (DGEMN). At that time the church was bought by the town hall and later, during the 1980s and 1990s, the church underwent conservation and rehabilitation interventions by DGEMN, which left it as it is nowadays.

The church presents a rectangular plant. Figure 14 indicates the dimensions of the church according to the latest survey performed by DGEMN. The church is composed by a single nave, a main arch that makes the transition to the main-chapel and a sacristy with square plant positioned on the South side of the main-chapel. There is a small bell stone structure on the top of the South wall, close to the main façade.

The church main supporting structures are two leaf stone masonry walls, approximately 1.0m thick, with an infill middle layer. The church roof (Fig. 15) is sustained by wooden trusses distant 0.45 m from each other and made by elements with rectangular cross-section, $(0.10 \times 0.12)\ m^2$. The trusses are connected on the inside of the church by a 2.0 cm thick wooden lining, and on the outside by the framework that supports the tiles. The roof structure is supported on the sides by the lateral walls. Since the trusses don't have bottom chords, they introduce horizontal transversal forces on the walls.

4.2 Numerical model

4.2.1 Geometric properties

The numerical models were created based on the geometrical surveys performed during the technical inspections to the church and on the most recent topographic elements found in DGEMN archives. This information was treated through a set of steps that involved auxiliary programs such as AutoCad (Autodesk 2002), GiD (CIMNE 2007) and a specially developed

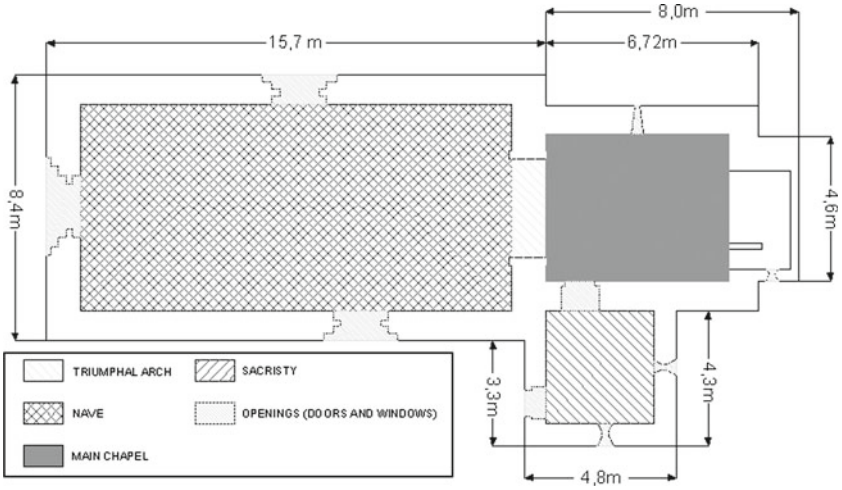

Fig. 14 The church implantation and space description

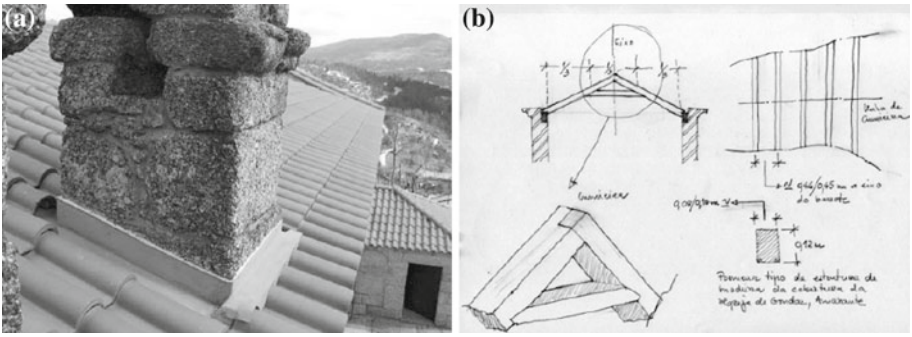

Fig. 15 The Gondar church roof: **a** outside view and **b** schematic drawing of the roof wooden structure by Augusto Costa, director of the former Regional Directorate of Buildings and Monuments of the North of Portugal

interface program, before being introduced in the finite elements program Cast3M (CEA 1990) used in this study.

Different strategies were used to simulate the church masonry walls, featuring different levels of geometrical complexity and detail. Thus, different types of finite elements and meshes were considered, giving rise to the geometrical models presented in Fig. 16 and described in Table 4. Although the foundation conditions and the soil-structure interaction may be relevant to the structure response, these aspects weren't taken into account in this study. The church was considered to be rigidly fixed at the basement.

4.2.2 Mechanical properties

The stone masonry behaviour was simulated using the continuum damage model and the parameters presented in Table 2. The elements of the roof structure were simulated using a linear elastic model with the mechanical characteristics presented in Table 5.

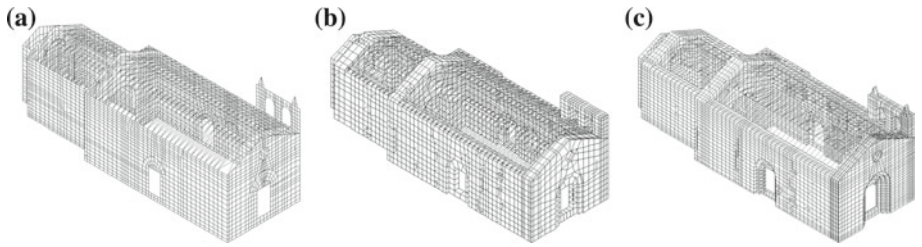

Fig. 16 Geometrical numerical models of the Gondar church: **a** MSC, **b** MSV and **c** MCV (see Table 2)

Table 4 Modelling strategies

Model	Geometry	Type of finite element	Type of material model
MSC-L	Simple	Shell (QUA4)	Linear (L)
MSV-L	Simple	Volume (CUB8)	Linear (L)
MSV-NL	Simple	Volume (CUB8)	Non Linear Damage (NL)
MCV-L	Complex	Volume (CUB8)	Linear (L)

Table 5 Wood elements mechanical characteristics

Material	$S_{\text{Wood}}\,(\text{m}^2)$	E_{Wood} (GPa)	$\rho_{\text{Wood}}\,(\text{kg/m}^3)$	ν_{Wood}
Oak	0.012	14.0	650.0	0.37

4.2.3 Modal analysis

Any dynamic study involves a modal analysis. It allows a better and more detailed knowledge of the structure dynamic characteristics, namely the vibration modes and frequencies. It also helps to define the integration time step for time integration analysis and to better understand the structure response when submitted to the seismic load.

The comparison of the modal analysis for the different geometrical models, MSC, MSV and MCV, showed almost no change on the structure's response. Figure 17 presents the first 10 main vibration modes involving the masonry walls of the model MSV. In addition to these modes, there were local vibration modes involving mainly the roof structure. Although these modes have an important local influence, they don't condition the global response. Thus, the roof was considered but not represented.

Comparing the results obtained with the two volumetric models, MSV and MCV, it was found that the simplifications adopted in the first model induced a decrease of approximately 3.0% in the roof mass and an increase of approximately 2.5% in the walls mass. As result of these small differences, the model MCV presented frequencies smaller than those of the model MSV for the same vibration modes. Comparing the shell model (MSC) with the volumetric models (MCV and MSV), the frequencies for the same vibration modes are lower than those obtained with the volumetric models, being this mainly due to the lower stiffness of the shell structure, especially at the walls intersections.

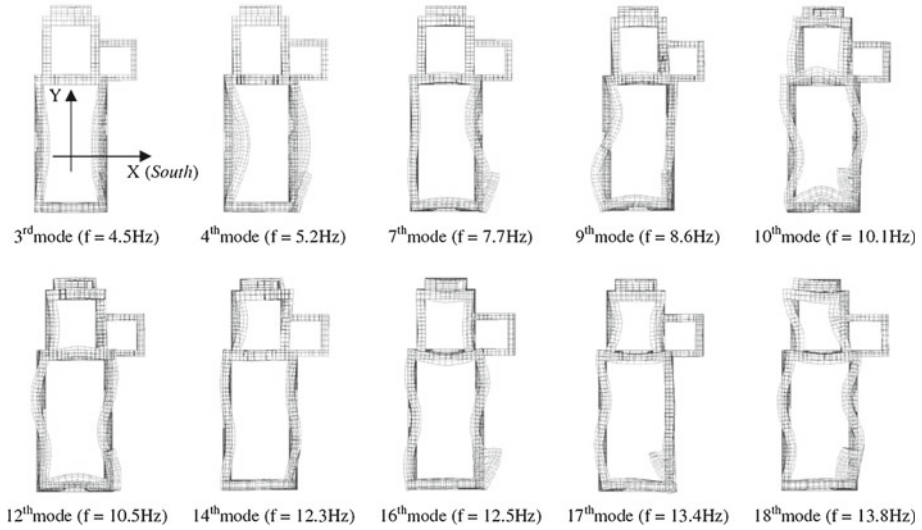

Fig. 17 Vibration modes and frequencies (MSV)

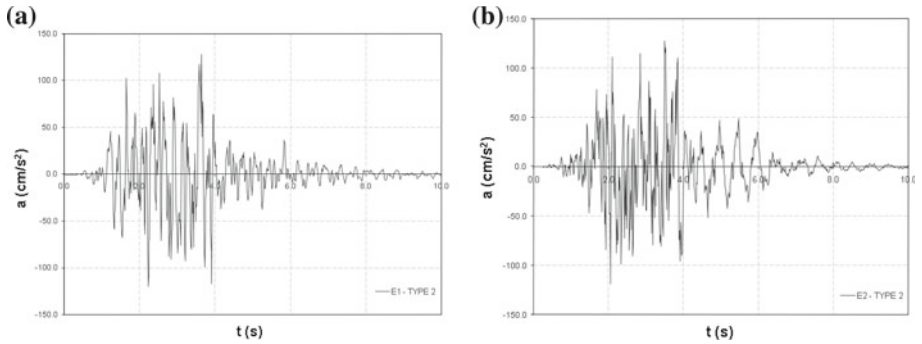

Fig. 18 Artificial accelerograms: **a** E1 and **b** E2

4.2.4 Loading conditions

The loads used on the assessment of the seismic behaviour of the Gondar church were the dead load (G_k) and the seismic loads (E_k). The dead load consisted on the weight of the walls and roof, and was computed internally by the program, based on the mechanical and geometrical properties of the materials.

The seismic analysis was performed using type 2 (near seismic action) artificial accelerograms (E_1 and E_2—Fig. 18) which proved, according to a preliminary modal analysis, to be more damaging for this type of structure. The accelerograms were generated according to the EC8 (CEN 2005) response spectrum and to the zoning proposed for Portugal. This particular structure is located in a level 5 zone and over a medium soil (type C), which corresponds to a maximum reference accelerations of 50 cm/s^2, for a type 1 seismic action, and 80cm/s^2 for a type 2 seismic action.

The accelerograms were generated using the program SIMQKE (Vanmarckle et al. 1969), and treated using an excel spreadsheet developed by Campos Costa (1993) that permits the visualization of the corresponding response spectra and the comparison to the normalized

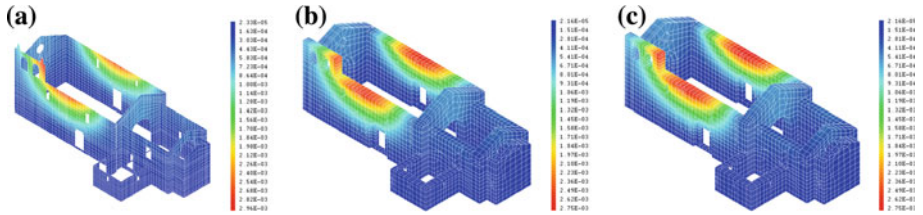

Fig. 19 Comparison of the maximum absolute displacements (cm) at the top of the nave lateral walls i.e., the main damaged concentration areas for dead loads: **a** MSC-L ($\text{Disp}_{max} = 0.29$ cm), **b** MSV-L ($\text{Disp}_{max} = 0.27$ cm) and **c** MSV-NL ($\text{Disp}_{max} = 0.28$ cm)

spectrum. The accelerogram E_1 was applied to both horizontal directions (XX and YY) and E_2 was applied to the vertical direction (ZZ), according to the following load combinations:

$$\text{Comb}_1 = G_k + (E_1)_X \tag{3}$$

$$\text{Comb}_2 = G_k + (E_1)_Y \tag{4}$$

$$\text{Comb}_3 = G_k + (E_1)_X + (0.9 \times E_2)_Z \tag{5}$$

$$\text{Comb}_4 = G_k + (E_1)_Y + (0.9 \times E_2)_Z \tag{6}$$

4.2.5 Static analysis

Before the dynamic analyses, a static analysis considering only the dead load was performed in order to determine the initial stress and deformation state. The results are presented next in terms of the maximum absolute displacements (Fig. 19) and of the maximum principal stresses (S_{11} and S_{33}—Fig. 20) for the three models: MSC, MSV-L and MSV-NL. The model MCV wasn't considered in this and in the successive analyses. It required computation time and storing capacity that made it impracticable, especially when the non linear material model was considered.

The analysis of these results shows that the different models present similar behaviour. Furthermore, the roof structure introduces important deformation at the top of the lateral walls, especially at the nave, pushing them to the exterior, Fig. 19. This out-of-plane flexure movement of the walls caused by the roof is the main responsible for the stresses concentration found in the structure: the main tensile stresses appear on the outer face of the nave lateral walls near the roof and on the inner face at the intersection of the nave walls; the main compression stresses are located on the outer face of the nave lateral walls near the base.

4.2.6 Seismic analysis

The seismic analysis performed on the three models (MSC, MSV-L and MSV-NL) showed, for both load combinations Comb_1 and Comb_2, similar stresses and deformations distribution. Figure 21 illustrates the church seismic response in terms of maximum absolute displacements and maximum principal stresses (S_{11} and S_{33}) for the model MSV-NL. Although similar distribution of stresses and deformations was found, the comparison of the different models shows that the highest displacement and stress values, in both dynamic and static conditions, were obtained with the model MSC-L due to the lower stiffness of this model in comparison to the volumetric models. In terms of the volumetric models, the model MSV-NL presented higher displacements than the model MSV-L, a result that is essentially due to the tensile damage that is taken into account by the continuum damage model. Notice

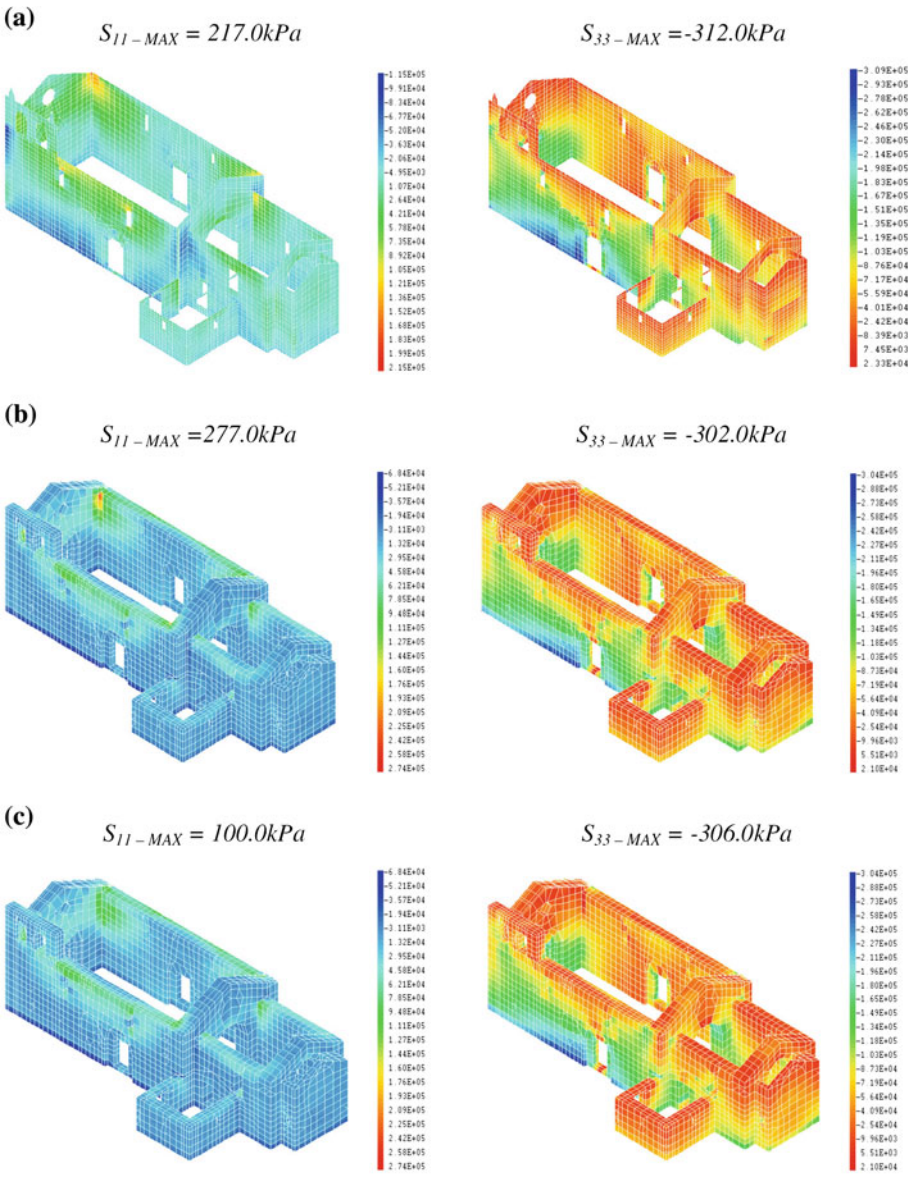

Fig. 20 Maximum tensile (S_{11}) and compression (S_{33}) principal stress maps (Pa) for the dead loads: **a** MSC, **b** MSV-L and **c** MSV-NL

that this model takes into consideration the accumulative development of damage (tensile and compressive), allowing a better understanding of damage progression along the masonry structures, in particular the way cracking and (or) joint openings spread.

Thus, the results with the model MSV-NL allows representing the church tensile damage maps $\left(d^{+}\right)$, which provide a better perception of how damage Fig. 22 presents the church tensile damage state for the two load combinations $Comb_1$ and $Comb_2$. For the load combination $Comb_1$, the main zones of damage concentration are at the lateral facades of the

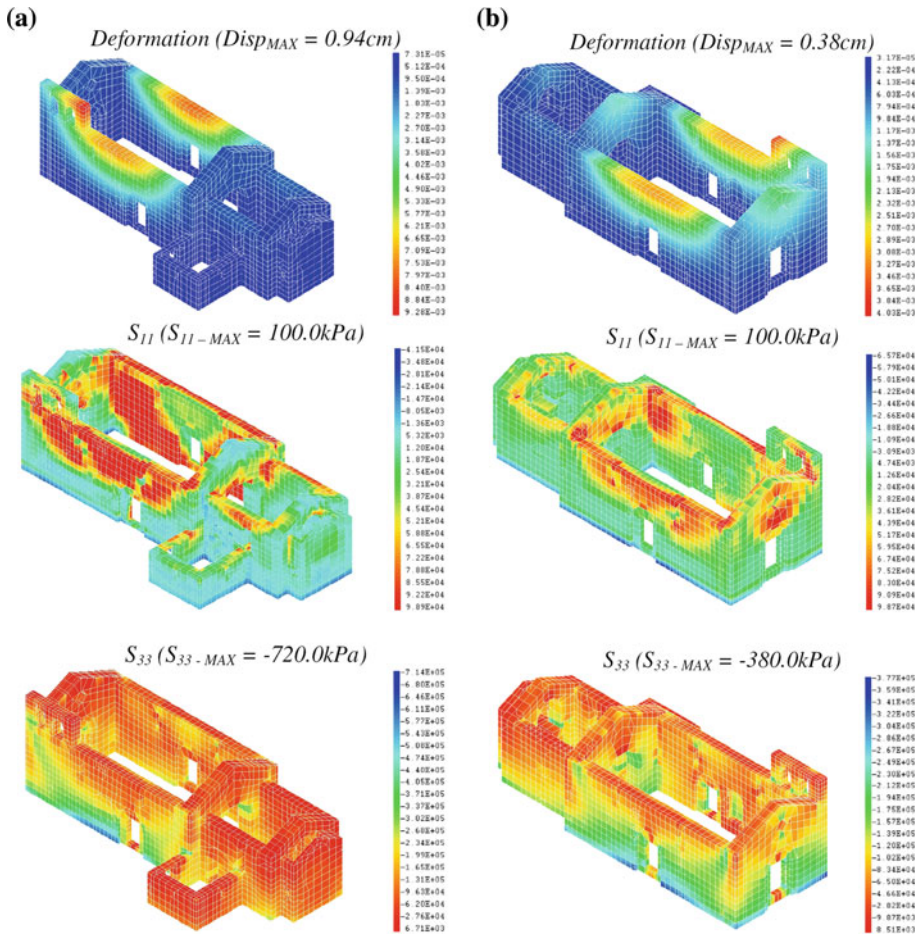

Fig. 21 Maximum absolute displacements (cm) and tensile (S_{11}) and compression (S_{33}) principal stress maps (Pa) for the model MSV-NL and for the load combinations: **a** $Comb_1$ and **b** $Comb_2$

nave. This is due to the out-of-plane flexure movement of the walls to the outside, as it is confirmed by the damage observed on the outer face near the roof and on the interior face along the flexure line. For the combination $Comb_2$, the main zones of damage concentration happen at the intersections of the walls and, in smaller extend, on the outer face of the lateral and frontal facades of the nave. These results give a good perception of the possible rupture mechanisms the structures may be submitted to.

The consideration of the seismic vertical component ($Comb_3$ and $Comb_4$) in this structure didn't introduce almost any alteration on the structural response in comparison with the results obtained with the load combinations $Comb_1$ and $Comb_2$. Therefore, they are not presented.

5 Conclusions

This work aimed the evaluation of the capacity of a non linear continuum damage model (Faria 1994), originally developed for concrete, to simulate the behaviour of stone masonry.

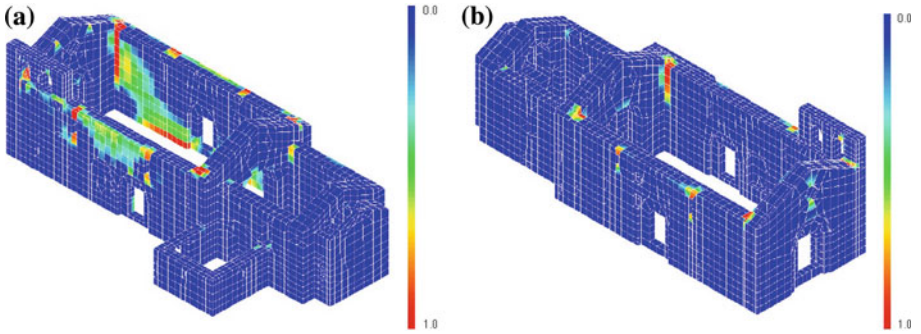

Fig. 22 Tensile damage maps (d^+) for the load combinations: **a** Comb_1 and **b** Comb_2

The verification and calibration procedures were performed using the experimental results from tests performed on stone masonry walls at the LESE and from other tests found in the literature (Vasconcelos 2005).

The experimental tests performed at the LESE allowed assessing the behaviour of this type of structures and the phenomena, local and global, involved when the walls are submitted to horizontal in-plane cyclic loads, namely: the walls deformation, the location of damage concentration areas (cracking and sliding) and the way damage develops along the structure. From a more global point of view, it was possible to assess global parameters such as the stiffness (loading, unloading and reloading trajectories), the energy dissipation and the resisting capacity of the walls.

The heterogeneity of this material commands the local behaviour observed in the tests; the results are quite sensitive to the way the stones and joints are distributed, with concentration of damage at the joints. However, at a global level the walls responded with great symmetry and uniformity, diluting many of the local particularities.

In what concerns the calibration of the continuum damage model based on the experimental results, it was concluded that although the model is capable of capturing the main global phenomena of stone masonry walls, the local behaviour, which is highly dependent on the geometrical features, can be hardly simulated with such a homogenous model. In particular, the model can't represent the sliding along the joints, which induces highly non linear shear behaviour.

The model calibration based on the results found in Vasconcelos (2005), when compared with the calibration using the experimental data gathered at the LESE, allowed a better approach in terms of energy dissipation. The axial force considered on the walls by Vasconcelos is higher, inducing a better fitting between the numerical and the experimental results. However, the same difficulties in the simulation of the unloading stiffness and of the energy dissipation were also observed in this case. This is mainly due to the inability of this damage model to capture phenomena related to the walls local behaviour, such as the joints friction.

On a second phase, the seismic response of an old stone masonry construction was analysed using different degrees of geometrical and material complexity. The results were compared, assessing the differences and the importance of using complex tools, such as the continuum damage model previously calibrated, to simulate the global behaviour of such constructions. The results obtained with the different numerical models and for the considered load combinations, showed similar damage, stress and deformation patterns, with major concentration

on the lateral facades of the nave due to the out-of-plane flexure movements to the exterior, induced by the roof and aggravated by the seismic load.

The use of the continuum material damage model allowed taking into consideration the accumulative development of the damage in the structure, in particular the tensile damage, allowing a more realistic simulation and a better understanding of the damage progression and of the possible mechanisms of rupture the structures may be submitted to.

References

Autodesk Inc (2002) http://usa.autodesk.com. AutoCAD

Berto L, Scotta R, Vitaliani V, Saetta A (2001) An orthotropic damage model for non linear masonry walls analysis: irreversible strain and friction effects. Structural Analysis of Historical Constructions, Guimarães, Portugal

Betti M, Orlando M, Vignoli A (2006) Modelling and analysis of an italian castle under earthquake loading: diagnosis and strengthening. Structural Analysis of Historical Constructions, New Delhi

Binda L, Modena C, Baronio G, Abbaneo S (1997) Repair and investigation techniques for stone masonry walls. Construct Build Mater 11(3):133–142

Campos Costa, APN (1993) A acção dos sismos e o comportamento das estruturas. PhD Thesis, Departamento de Engenharia Civil, Faculdade de Engenharia da Universidade do Porto. Porto, Portugal

CEA (1990) Visual Cast3M—Guide d' utilisation, France

CEN (2005) Eurocode 8: Design of structures for earthquake resistance. EN 1998 1:2005, Part 1

Cervera, M (2003) Viscoelasticity and rate-dependent continuum damage models. Monograph M79, CIMNE. Barcelona, Spain

CIMNE (2007) http://gid.cimne.upc.es/index.html. GiD

Corradi M, Borri A, Vignoli A (2002) Strengthening techniques tested on masonry structures struck by the Umbria-Marche earthquake of 1997–1998. Construct Build Mater 16(4):229–239

Corradi M, Borri A, Vignoli A (2003) Experimental study on the determination of strength of masonry walls. Construct Build Mater 17(5):325–337

Costa C (2004) Implementação do modelo de dano em tracção e compressão com plasticidade no programa Cast3M, Laboratório ELSA

Costa AA, Silva B, Costa A, Guedes J, Arêde A (2006) Structural behaviour of a masonry wall under horizontal cyclic load; experimental and numerical study. Structural Analysis of Historical Constructions, New Delhi

Costa AA, Arêde A, Costa A, Oliveira CS (2010) In-situ cyclic tests on existing stone masonry walls and strengthening solutions. Earthq Eng Struct Dyn (in press)

Faria R (1994) Avaliação do comportamento sísmico de barragens de betão através de um modelo de dano contínuo. PhD Dissertation, Departamento de Engenharia Civil, Faculdade de Engenharia da Universidade do Porto. Porto, Portugal

Faria R, Oliver J, Cervera M (1998) A strain-based plastic viscous-damage model for massive concrete structures. Int J Solids Struct 35(14):1533–1558

Gambarotta L, Lagomarsino S (1997) Damage models for the seismic response of brick masonry shear walls. Part I: the mortar joint model and its applications. Earthq Eng Struct Dyn 26:423–439

Gambarotta L, Lagomarsino S (1997) Damage models for the seismic response of brick masonry shear walls. Part II: the continuum model and its applications. Earthq Eng Struct Dyn 26:441–462

Lourenço PB, Rots JG (1997) A multi-surface interface model for the analysis of masonry structures. J Eng Mech ASCE 123(7):660–668

Lourenço PB, de Borst R, Rots JG (1997) A plane stress softening plasticity model for orthotropic materials. Int J Numer Methods Eng 40:4033–4057

Penazzi D, Valluzzi MR, Saisi A, Binda L, Modena C (2001) Repair and strengthening of historic masonry buildings in seismic areas. International Congress. More than Two Thousand Years in the History of Architecture Safeguarding the Structure of our Architectural Heritage, pp 1–6. Bethlehem, Palestine

Roque JCA (2002) Reabilitação estrutural de paredes antigas de alvenaria. MSc Thesis, Universidade do Minho. Guimarães, Portugal

Saetta A, Scotta R, Vitaliani R (2000) An orthotropic Fourth-Rank Damage Model for Masonry Structures. European Congress on Computational Methods in Applied Sciences and Engineering, ECOMAS 2000. Barcelona, Spain

Silva B, Guedes J, Arêde A, Costa A (2007) Avaliação experimental do comportamento estrutural de uma parede de alvenaria de pedra não reforçada sob acção cíclica. SÍSMICA 2007—7º Congresso de Sismologia e Engenharia Sísmica, Porto, Portugal

Tomaževic M (1992) Laboratory and in-situ tests of the efficacy of grouting and tying of stone masonry walls. In International workshop on the Effectiveness of injection techniques for retrofitting of stone and brick masonry walls in seismic areas, Politecnico di Milano, pp 95–116

Valluzzi MR, Binda L, Modena C (2001) Experimental and analytical studies for the choice of repair techniques applied to historic buildings. Matériaux et Constructions (CD-ROM), RILEM

Valluzzi MR, Cardani G, Binda L, Modena C (2004) Analysis of the seismic vulnerability of masonry buildings in historical centres and intervention proposals. 6th International symposium on the conservation of monuments in the mediterranean Basin, Lisbon, Portugal

Vanmarckle CH, Cornell CA, Gasparini DA, Hou SN (1969) SIMQKE: simulation of earthquake ground motion. MIT, Cambridge, MA

Vasconcelos G (2005) Experimental investigations on the mechanics of stone masonry: characterization of granites and behaviour of ancient masonry shear walls. PhD Thesis, Universidade do Minho, Guimarães, Portugal

Vicente R, Varum H, Mendes da Silva JAR, Lagomarsino S, Parodi S (2007) Metodologia de avaliação da vulnerabilidade sísmica de edifícios antigos à escala do centro histórico. SÍSMICA 2007—7º Congresso de Sismologia e Engenharia Sísmica, Porto, Portugal

Vintzileou E, Tassios TP (1995) Three leaf stone masonry strengthened by injecting cement grouts. J Struct Eng 848–856